

Hydrothermal Synthesis and Characterization of PEG-Mn₃O₄ Nanocomposite

E. Karaoğlu^{1*}, H. Deligöz², H. Sözeri³, A. Baykal¹, M. S. Toprak⁴

(Received 14 Nov. 2010; accepted 16 Mar. 2011; published online 19 April 2011.)

Abstract: Here, we report on the synthesis of PEG-Mn₃O₄ nanocomposite (NP's) via a hydrothermal route by using Mn(acac)₂, ethanol, NH₃ and PEG-400. The crystalline phase was identified as Mn₃O₄. The crystallite size of the PEG-Mn₃O₄ nanocomposite was calculated as 12±5 nm from X-ray line profile fitting and the average particle size from TEM was obtained as 200 nm. This reveals polycrystalline character of Mn₃O₄ NP's. The interaction between PEG-400 and the Mn₃O₄ NP's was investigated by FTIR. Temperature independent AC conductivity of PEG-Mn₃O₄ nanocomposite beyond 20 kHz provides a strong evidence of ionic conduction through the structure. The conductivity and permittivity measurements strongly depend on the secondary thermal transition of nanocomposite beyond 100°C. Above that temperature, Mn₃O₄ particles may interact with each other yielding a percolated path that will facilitate the conduction. On the other hand, the relatively lower activation energy ($E_a=0.172$ eV) for relaxation process suggests that polymer segmental motions of PEG and electrons hopping between Mn²⁺ and Mn³⁺ may be coupled in the sample below 100°C. Room temperature magnetization curve of the sample does not reach to a saturation, which indicates the superparamagnetic character of the particles. As the temperature increases, the frequency at which (ϵ'') reaches a maximum shifted towards higher frequencies. The maximum peak was observed at 1.4 kHz for 20°C while the maximum was detected at 23.2 kHz for 90°C.

Keywords: Spinel; Magnetic nanomaterials; Conductivity; Magnetic properties; Hydrothermal Synthesis

Citation: E. Karaoğlu, H. Deligöz, H. Sözeri, A. Baykal and M. S. Toprak, "Hydrothermal Synthesis and Characterization of PEG-Mn₃O₄ Nanocomposite", Nano-Micro Lett. 3 (1), 25-33 (2011). <http://dx.doi.org/10.3786/nml.v3i1.p25-33>

Introduction

Among magnetic nanoparticles, manganese oxide (Mn₃O₄) as a magnetic transition-metal oxide is an important material. It has a wide range of applications as catalyst, ion-exchange medium, molecular adsorbent, and in electrochemical materials and varistors [1-5]. Furthermore, Mn₃O₄ has been widely used as the main source of ferrite materials, finding extensive applications in electronics and information technologies. Mn₃O₄ is known to crystallize in the normal spinel

structure with a tetragonal distortion elongated along the c-axis. Manganese ions are located in the tetrahedral A-sites (Mn²⁺) and octahedral B-sites (Mn³⁺).

Mn₃O₄ with various forms and shapes, such as nanocomposites [6], nanorods [7], nanowires [8], tetragonal [9] and polyhedral nanocrystals [3], has been synthesized. Several methods, such as solvothermal / hydrothermal [10,11], vapor phase growth [12], vacuum calcining precursors [13], thermal decomposition [14], ultrasonic, gamma and microwave irradiation [15-17], chemical liquid homogeneous precipitation [18], and

¹Department of Chemistry, Fatih University, 34500 B. Cekmece- Istanbul/Turkey

²Chemical Engineering Department, Istanbul University, 34320 Avcılar-Istanbul/Turkey

³TUBITAK-UME, National Metrology Institute, Gebze, 41470 Kocaeli/Turkey

⁴Division of Functional Materials, Royal Institute of Technology, 16440 Stockholm/Sweden

*Corresponding author. Tel: +91 212 866 33 00 Ext.2070; Fax: +90 212 866 34 02

E-mail address: ekaraoglu@fatih.edu.tr (E.Karaoglu)

polyol synthesis [19] processes have been developed for the synthesis of Mn_3O_4 NP's.

In order to obtain monodisperse nanocomposites, different kinds of stabilizers have been utilized, including polymers, dendrimers, surfactants and other ligands, to overcome the van der Waals interaction between the nanoclusters which otherwise lead to agglomeration [20]. For long-term stability, researchers often employ surfactants as either stabilizers or templates in the synthesis to decrease the surface energy, control the growth and shape of the particles, and act against aggregation [20]. It has been reported that PEG with a uniform and ordered chain structure is easily absorbed at the surface of metal oxide colloid [21]. When the surface of the colloid adsorbs this type of polymer, the activities of colloid greatly decrease and the growth rate of the colloids in some certain facet will be confined [22,23]. Therefore, the addition of PEG in the metal oxide colloids will modify the growth kinetics of the growing colloids, which finally, leads to anisotropic growth of the crystals. For this reason, linear PEG has been widely used in the synthesis of a series of nanoparticulates and 1D materials in solution [22].

Polymeric materials decorated with inorganic nanoparticles are of particular interest because possible interactions between the inorganic nanoparticles and the polymer matrices may generate some unique physical properties upon the formation of various micro/nanocomposites [24-27]. Recently, interesting research has been focused on the polyaniline-inorganic nanocomposites to obtain the materials with synergistic or complementary behavior between polyaniline and inorganic nanoparticles [28-31].

Here, we report on the synthesis of PEG- Mn_3O_4 nanocomposite. This is, so far, the first report using the adopted route for the synthesis of a PEG- Mn_3O_4 nanocomposite. Results of comprehensive physico-chemical and magnetic characterization are presented.

Experimental

Chemicals and Instrumentation

All chemicals ($\text{Mn}(\text{acac})_2$, NH_3 , PEG-400, absolute ethanol) were analytical grade and were used without further purification.

X-ray powder diffraction (XRD) analysis was conducted on a Rigaku Smart Lab Diffractometer operated at 40 kV and 35 mA using $\text{Cu-K}\alpha$ radiation ($\lambda=1.54178 \text{ \AA}$).

Fourier transform infrared (FT-IR) spectra were recorded in transmission mode, in the range $4000\sim 400 \text{ cm}^{-1}$, with a Perkin Elmer BX FT-IR infrared spectrometer. The powder samples were ground with KBr and compressed into a pellet prior to analysis.

Transmission electron microscopy (TEM) analysis

was performed using a JEOL JEM 2100 microscope. A drop of diluted sample in alcohol was dripped on a carbon coated Cu TEM grid.

The thermal stability was determined by thermogravimetric analysis (TGA, Perkin Elmer Instruments model, STA 6000). The TGA thermograms were recorded for 5 mg of powder sample at a heating rate of 10°C per min, in the temperature range of $30^\circ\text{C}\sim 700^\circ\text{C}$ under nitrogen atmosphere.

VSM measurements were performed by using a Quantum Design Vibrating Sample Magnetometer (QD-VSM). The sample was measured between ± 15 kOe at room temperature. The electrical characterizations, AC conductivity and dielectric properties of PEG- Mn_3O_4 nanocomposite were measured by using Novocontrol dielectric impedance analyzer in the frequency range of $1 \text{ Hz}\sim 3 \text{ MHz}$. The samples were used in the form of circular pellets of 13 mm diameter and 3 mm thickness and the pellets were sandwiched between gold electrodes (two probe through plane). The temperature was controlled with a Novocontrol Cryosystem between 20 to 120°C . The dielectric data (ϵ' and ϵ'') were collected during heating as a function of frequency.

Procedure

In a typical experiment, 1 g of $\text{Mn}(\text{acac})_2$ was added dropwise into three-neck round-bottom flask. Then 16.7 ml PEG-400, heated and melted, was injected to the flask under NH_3 gas (pH=11). After continuous stirring, a homogeneous solution could be obtained. Then it was put in the autoclave and was kept at 160°C for 12 h, then cooled to room temperature naturally. The products were filtered and washed several times with distilled water and absolute ethanol, and finally dried in a vacuum oven at 60°C for 12 h.

Results and Discussion

XRD Analysis

XRD patterns of prepared samples are shown in Fig. 1. The characteristic peaks at 2θ angles correspond very well to the standard card of Mn_3O_4 (JCPDS Card No. 18-0803), which proves that the samples can be identified as Mn_3O_4 . The mean size of the crystallite was also estimated from the diffraction pattern by line profile fitting method using the Eq. (1) given in Refs. [32,33]. The line profile, shown in Fig. 1, was fitted for the observed 12 peaks with the following miller indices: (101), (112), (200), (103), (211), (004), (220), (105), (312), (321), (224), and (400). The average crystallite size D was obtained as $12 \pm 5 \text{ nm}$ as a result of this line profile fitting.

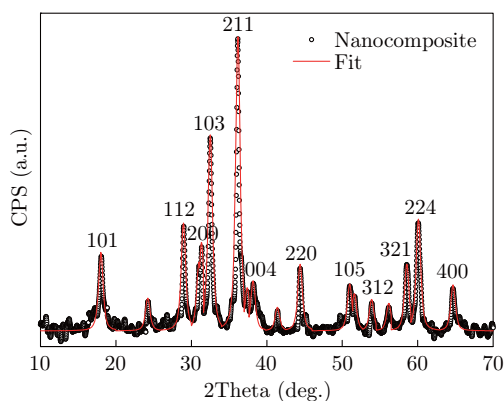


Fig. 1 XRD powder pattern of PEG-Mn₃O₄ nanocomposite.

FTIR Analysis

In order to assess the interaction between the PEG and the nanoparticles, FTIR analysis of PEG as well as PEG-Mn₃O₄ nanoparticles was performed; and the spectra are presented in Fig. 2. Vibrations of ions in the crystal lattice are usually observed in the range of 1000 ~ 400 cm⁻¹ in FTIR analysis. Two main broad metal-oxygen bands are seen in the FTIR spectra of all spinels, and ferrites in particular. The highest one, ν_1 , generally observed in the range 600~500 cm⁻¹, corresponds to intrinsic stretching vibrations of the metal at the tetrahedral site (T_d), M_{tetra} ↔ O, whereas the ν_2 - lowest band usually observed in the range 450 ~ 385 cm⁻¹, is assigned to octahedral-metal stretching (O_h), M_{octa} ↔ O[2][4] [34-37] (see Fig. 2(a)). Due to the limitation of our FTIR instrument below 400 cm⁻¹, ν_3 (328 cm⁻¹) and ν_4 (below 300 cm⁻¹) were not detected. The FTIR measurements reveal that the vibrational band of C-O bond shifts from 1113 cm⁻¹ for pure ethylene glycol to 1095 cm⁻¹ for the current Mn₃O₄

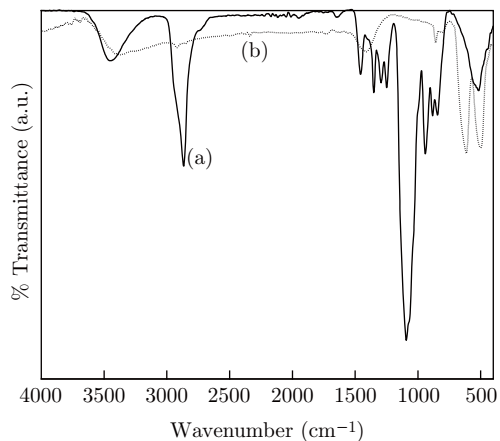


Fig. 2 FTIR spectra of (a) PEG-400, and (b) PEG-Mn₃O₄ nanocomposite.

nanoparticles, which indicates that the O from C-O coordinates with metal on the surface of Mn₃O₄ nanoparticles. Similarly, the bands around 2910 cm⁻¹ and 955 cm⁻¹ corresponded to -CH₂ stretching vibrations and -CH out of plane bending vibrations, respectively (as shown in Fig. 2(b)). The presence of -CH₂ and -CH peaks were strong evidence that PEG was chemically bonded to the surface. The surfactant molecules in the adsorbed state are influenced by the field of solid-state surface. As a result, the characteristic bands shifted to a lower frequency region (see Fig. 2(a)) [38,39].

Morphological Analysis

TEM micrographs of PEG-Mn₃O₄ nanocomposite are shown in Fig. 3(a) and the particle size distribution obtained thereof is presented in Fig. 3(b). Particles are observed to have spherical morphology and seem to be aggregated probably due to the polymer coating. Size distribution histogram is obtained by measuring at least 150 nanoparticles and is fitted by using a log-normal function. An average size, D_{TEM/log-normal}, of about 200 nm was obtained for magnetite nanoparticles. Crystallite size obtained from XRD line profile fitting is much smaller than the particle size estimated from TEM, revealing polycrystalline nature of Mn₃O₄ nanoparticles. Polymer PEG coating on nanoparticles, however, is still not detectable via this imaging technique.

Thermal analysis

TG analysis

Thermal stability of the precursor powder and final powder has been analyzed using TGA (see Fig. 4). To further confirm the existence of PEG on the surface of Mn₃O₄ nanoparticles and quantify the proportion of organic and inorganic phase, TGA was performed in the temperature range of 30~700°C. Pure PEG combustion started at about 340°C and completely combusted at about 420°C [40] (see Fig. 4(a)). Evidently, the combustion is delayed for the PEG capped Mn₃O₄ nanoparticles, which start at about 380°C and complete at about 410°C. The increase of combustion temperature is due to the extra interaction between the PEG and Mn₃O₄ nanoparticles [41,42]. Product shows a major weight loss of about 20% over the temperature range of 30~700°C due to the decomposition and combustion of PEG (see Fig. 4(b)). This implies that product has almost 80% inorganic phase as Mn₃O₄ nanoparticles.

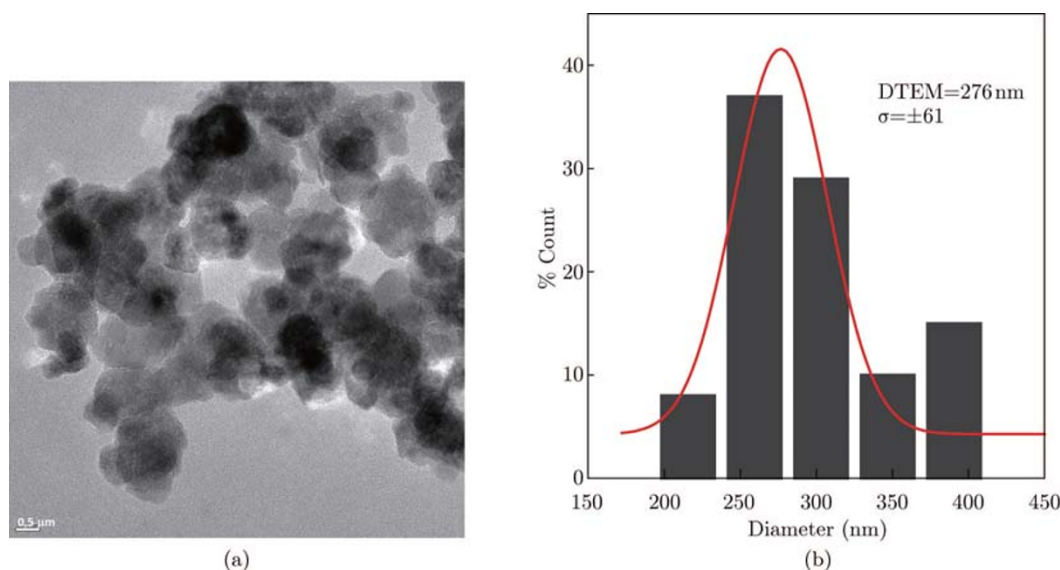


Fig. 3 (a) TEM micrographs of PEG-Mn₃O₄ nanocomposite, and (b) size distribution histogram obtained thereof.

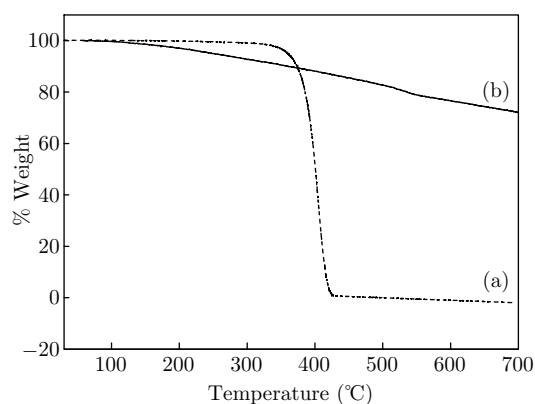


Fig. 4 TGA curves of (a) PEG-400, and (b) PEG-Mn₃O₄ nanocomposite.

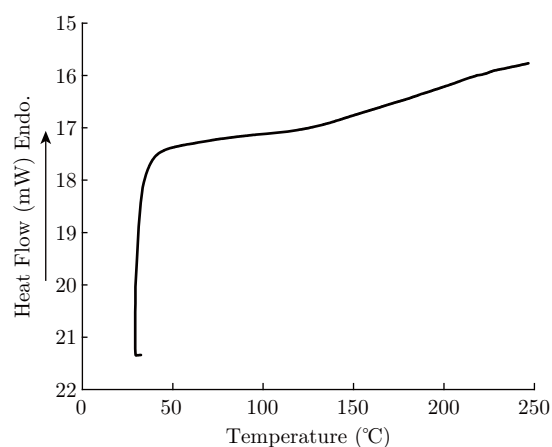


Fig. 5 DSC graph of PEG-Mn₃O₄ nanocomposite.

DSC analysis

To observe the glass transition of PEG-Mn₃O₄ nanocomposite, DSC analysis of the nanocomposite was performed and the obtained graph was given below (see Fig. 5). From DSC thermograph of nanocomposite, T_g of nanocomposite was found to be nearly 110°C and this can explain significant increase in AC conductivity of the nanocomposite between 100°C and 120°C due to the secondary phase transition of nanocomposite as other reviewers have pointed out. We do not expect a breakdown mechanism.

Magnetization

Magnetic characterization of the sample has been performed at room temperature by measuring M (H) hysteresis curves up to magnetic field

of ± 15 kOe (see Fig. 6). It is observed that magnetization increases almost linearly with the field, i.e., paramagnetic-like behavior, and does not saturate even at the maximal applied field. Besides, sample exhibits small coercivity, which indicates that there is ferromagnetic ordering in magnetization of the samples. Therefore, total magnetization can be described as $M(T, H) = \chi_P(T)H + M_F$, where $\chi_P(T)$ is the paramagnetic susceptibility, H is the magnetic field and M_F is the high-temperature ferromagnetic component of magnetization. M_F was determined as approximately 0.3 emu/g from the intercept of the hysteretic part with the linear one in Fig. 6. If we consider the bulk magnetization of Mn₃O₄ as 38 emu/g [3], we can deduce that sample has an impurity phase of nearly 0.8% from the ratio of saturation magne-

tization values of ferromagnetic and paramagnetic parts. Mn_3O_4 , which belongs to spinel oxides having the general form of AB_2O_4 with Mn^{2+} ions at A-sites and Mn^{3+} ions at B-sites, exhibits three distinct magnetic transitions. The ferromagnetic ordering occurs at $T_N=42$ K and at lower temperatures, Mn_3O_4 undergoes a transition to an incommensurate phase at 40 K and a transition to a commensurate phase at 34 K [43]. Therefore, the hysteretic behavior observed in our sample can only be explained by the presence of small fraction of the impurity phase but not with the intrinsic magnetic interactions.

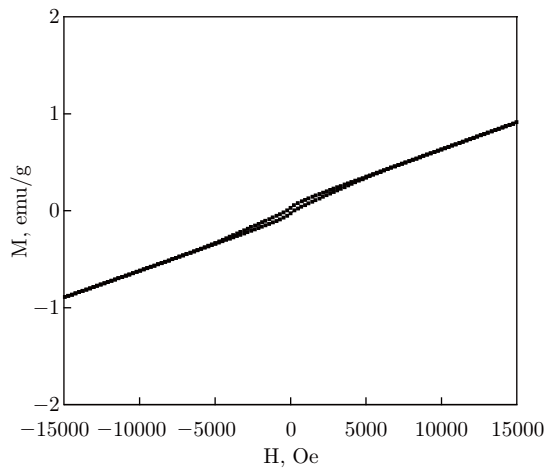


Fig. 6 Room temperature M-H curve for PEG- Mn_3O_4 nanocomposite.

Temperature and frequency dependent conductivity and dielectric permittivity measurements

The frequency and temperature dependent AC conductivity and dielectric permittivity (dielectric constant and dielectric loss) properties of PEG- Mn_3O_4 nanocomposite are studied over a broad frequency and temperature range. The related figures and explanations are given below.

AC conductivity

The AC conductivity of the PEG based nanocomposite including Mn_3O_4 was measured from 20 to 120°C using impedance spectroscopy as a function of frequency and temperature. The frequency-dependent AC conductivity graph is shown in Fig. 7. As well known, AC conductivity values were obtained using the following standard equation [44].

$$\sigma'(\omega) = \sigma_{ac}(\omega) = \varepsilon'' \sigma(\omega) \omega \varepsilon_0 \quad (1)$$

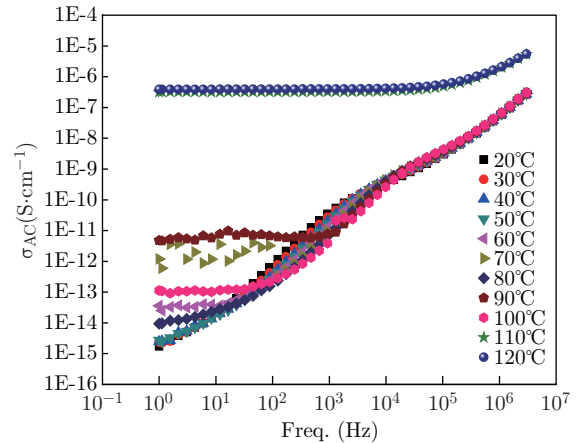


Fig. 7 The variation of AC conductivity of Mn_3O_4 including PEG- Mn_3O_4 nanocomposite as a function of frequency and temperature.

Where (ω) is the real part of conductivity, $\omega(2\pi f)$ is the angular frequency of the signal applied to the samples, ε'' is the imaginary part of complex dielectric permittivity and ε_0 (8.852×10^{-14} F/cm) is the vacuum permittivity.

The AC conductivity of nanocomposite including Mn_3O_4 nanoparticles showed two different behaviors depending on both temperature and frequency. Regarding the temperature dependency of nanocomposite, the conductivity values were very low and in the range of 10^{-15} to 10^{-12} S/cm up to 100°C. Beyond this temperature, the conductivity has remarkably increased (more than 10^4 times) and reached to the level of conductivity of 10^{-7} S/cm. It can be seen from Fig. 7 that the AC conductivities of PEG- Mn_3O_4 nanocomposite at 1 kHz were 1.25×10^{-15} S/cm and 3.67×10^{-7} S/cm for 20 and 120°C, respectively, which show the conductivity increases with temperature. This significant improvement in conductivity with temperature can be directly attributed to the secondary phase transition of nanocomposite. Beyond this temperature, Mn_3O_4 particles may interact with each other leading to a percolated path, which will facilitate the ionic conduction. This result shows that electrical current flows through both the semi-conducting Mn_3O_4 particles and dielectric PEG with the temperature range applied as reported earlier [44,50].

Concerning frequency dependence of AC conductivity, PEG- Mn_3O_4 nanocomposite exhibits a frequency-dependent conductivity at lower temperatures and frequencies. Interestingly it was ob-

served that the conductivity values are nearly the same beyond 20 kHz, independent of temperature, while nanocomposite exhibited a temperature-dependent behavior at low frequencies. This phenomenon can be considered as a strong clue for ionic conductivity.

Frequency and temperature dependence of dielectric constant (ϵ')

The dielectric constant (ϵ') of PEG-Mn₃O₄ nanocomposite is given in Fig. 8. The dielectric constant of the nanocomposite decreases with increasing frequency when temperature is kept constant. Furthermore, these curves keep their shapes but slide up at higher temperatures. These are well in agreement with thermosets and cross-linked polymers formerly reported in the literature [45,46]. Dielectric constants of polymers, in general, are known to decrease gradually with increasing frequency and similar behavior was observed for PEG-Mn₃O₄ nanocomposites prepared in this study. This behavior can be attributed to the frequency dependence of the polarization mechanisms. The dielectric constant depends upon the ability of the polarizable units in a polymer to orient fast enough to keep up with the oscillations of an alternating electric field. When frequency increases the orientational polarization decreases since the orientation of dipole moments need a longer time than electronic and ionic polarizations do. This causes the dielectric constant to decrease. Furthermore, the increase of (ϵ') towards the low frequency region is also seen from Fig. 8. This may be attributed to the blocking of charge carriers at the electrodes [47]. For example, ϵ' values of nanocomposite were found to be 1.12 and 1.35 for 1 MHz and 100 Hz, respectively.

Figure 8 also shows the variation of the dielectric constant (ϵ') depending on temperature interval of 20~120°C for the nanocomposite product. As known, the dielectric constant of polar polymers such as PEG increases with increasing temperature due to the molecular orientation and arrangement [48]. It is clearly emphasized in Fig. 8 that (ϵ') of the Mn₃O₄ nanocomposite increases with temperature due to the enhancement of interfaces between Mn₃O₄ and nonconductive polymer matrix as reported in literature [49]. Another interesting result can be seen from Fig. 8, the dielectric

constant of nanocomposite markedly increases beyond 100°C. This result can be explained by the secondary phase transition of nanocomposite. At this temperature, chemically bonded PEG based nanocomposite behaves as rubber-like and Mn₃O₄ particles may easily interact with each other yielding a percolated path that will facilitate the conduction. Hence, this can cause a significant increase in dielectric constant above 100°C. The ϵ' value of nanocomposites was found to be 24.4 at 100 Hz and 120°C while the dielectric constant was 1.35 at the same frequency and 100°C.

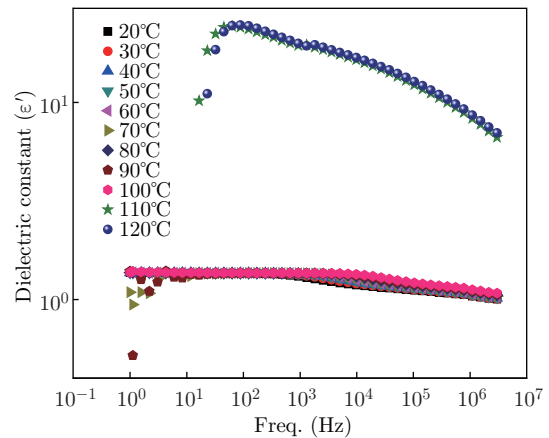


Fig. 8 The dielectric constant (ϵ') changes of PEG-Mn₃O₄ nanocomposite depending on temperature and frequency.

Frequency and temperature dependence of dielectric loss (ϵ'')

Figure 9 shows the dielectric loss (ϵ'') variations dependent on the frequency applied at different temperatures for PEG-Mn₃O₄ nanocomposites. It was observed that (ϵ'') increases as the frequency increases, reaches a maximum and thereafter decreases at 20~100°C temperature interval for nanocomposite. As the temperature increases, the frequency at which (ϵ'') reaches a maximum shifted towards higher frequencies. The maximum peak was observed at 1.4 kHz for 20°C while the maximum was detected at 23.2 kHz for 90°C. On the other hand, no shifting curve was found for the samples measured at 110 and 120°C. This is probably due to the being out of frequency range applied in the study. Conclusively, as the temperature increase, the frequency at which ϵ'' reaches a maximum shifted towards higher frequencies.

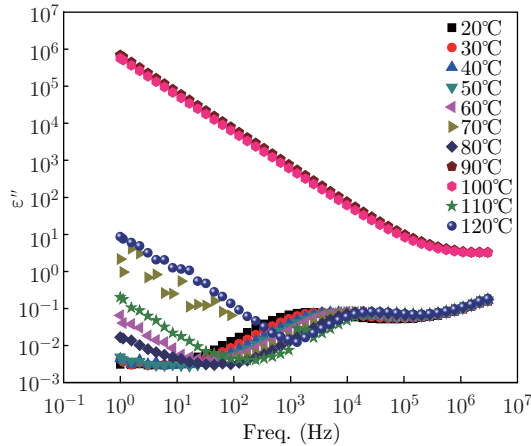


Fig. 9 The dielectric loss (ϵ'') changes of PEG-Mn₃O₄ nanocomposite depend on temperature and frequency.

In addition, the activation energy for the observed relaxation process was evaluated from the following equation.

$$\omega_{\max} = \omega_0 \cdot \exp(\Delta E/k_B T)$$

Where ω_{\max} is the frequency at which ϵ'' (tan dissipation) is maximum, k_B is Boltzmann's constant ($\text{eV} \cdot \text{K}^{-1}$), T is temperature in Kelvin degrees and ΔE is the activation energy. The plot of $\log(\omega_{\max})$ vs. $1/T$ is shown in Fig. 10. From the slope of the straight line, one evaluated activation energy was found to be 0.172 eV. This value of activation energy less than 1 eV indicates the predominance of electronic polarization at present. It is believed that this behavior can be explained as follows. The dielectric permittivity of nanocomposite suggests that polymer segmental motions of PEG and electron hopping between Mn^{2+} and Mn^{3+} may be coupled in the sample at lower temperatures than 100°C. Similar results were reported from ferrite

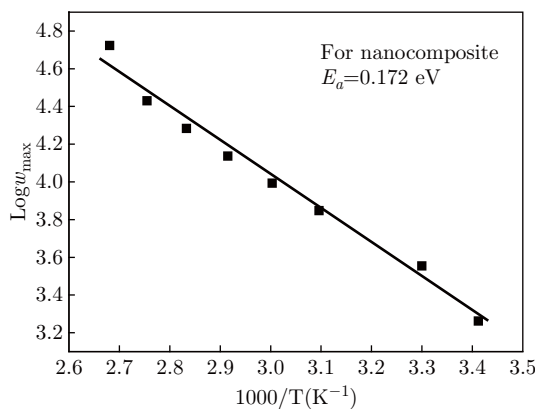


Fig. 10 $\text{Log}(\omega_{\max})$ vs. inverse absolute temperature of PEG-Mn₃O₄ nanocomposite.

containing nanocomposites in our recent articles [44,50].

Conclusion

We report on the synthesis of PEG-Mn₃O₄ nanocomposite via a hydrothermal route. The crystalline phase, identified as Mn₃O₄, was shown to have a crystallite size of 12 ± 5 nm from X-ray line profile fitting. Average particle size from TEM was obtained as 200 nm, which reveals polycrystalline character of Mn₃O₄ nanoparticles. The interaction between PEG-400 and the Mn₃O₄ nanoparticles was assessed to be via carbonyl groups coordination. Temperature independent AC conductivity of PEG-Mn₃O₄ nanocomposite beyond 20 kHz provides a strong evidence of ionic conduction through the structure. The conductivity and permittivity measurements strongly depend on the secondary thermal transition of nanocomposite beyond 100°C. Above that temperature, Mn₃O₄ particles may interact with each other yielding a percolated path that will facilitate the conduction. As the temperature increases, the frequency at which (ϵ'') reaches a maximum shifted towards higher frequencies. The maximum peak was observed at 1.4 kHz for 20°C while the maximum was detected at 23.2 kHz for 90°C. Besides, the relatively lower activation energy ($E_a=0.172$ eV) for relaxation process suggests that polymer segmental motions of PEG and electrons hopping between Mn^{2+} and Mn^{3+} may be coupled in the sample below 100°C.

Acknowledgements

The authors are thankful to the Fatih University, Research Project Foundation (Contract No.: P50020902-2) and Turkish Ministry of Industry and TUBITAK (Contract No.: 110T487) for financial support of this study. Authors also offer their special thank to Dr. Özgür DUYGULU for TEM measurements.

References

- [1] A. R. Armstrong and P. G. Bruce, Nature 381, 499 (1996). <http://dx.doi.org/10.1038/381499a0>.

- [2] T. Özkaya, A. Baykal and M. S. Toprak, *Cent. Eur. J. Chem.* 6, 465 (2008).
- [3] T. Ozkaya, A. Baykal, H. Kavas, Y. Köseoğlu and M. S. Toprak, *Physica. B* 403, 3760 (2008). <http://dx.doi.org/10.1016/j.physb.2008.07.002>
- [4] Z. Durmus, H. Kavas, A. Baykal and M. S. Toprak, *Cent. Eur. J. Chem.* 7, 555 (2009). <http://dx.doi.org/10.2478/s11532-009-0049-4>
- [5] Z. Durmus, A. Baykal, H. Kavas, M. Direkçi and M. S. Toprak, *Polyhedron* 28, 2119 (2009). <http://dx.doi.org/10.1016/j.poly.2009.03.026>
- [6] A. Vazquez-Olmos, R. Redon, G. Rodriguez-Gattorno, M. E. Mata-Zamora, F. Morales-Leal, A. L. Fernandez-Orosio and J. M. Saniger, *J. Colloid Interf. Sci.* 291, 175 (2005).
- [7] D. Portehault, S. Cassaignon, E. Baudrin and J. P. Jolivet, *J. Mater. Chem.* 19, 2407 (2009). <http://dx.doi.org/10.1039/b816348k>
- [8] E. Winkler, R. D. Zysler and D. Fiorani, *Phys. Rev. B* 70, 174406 (2004).
- [9] Z. Fang, K. Tang, L. Gao, D. Wang, S. Zeng and Q. Liu, *Mater. Res. Bull.* 42 (2007) 1761. <http://dx.doi.org/10.1016/j.materresbull.2006.11.025>
- [10] C. Feldmann, *Adv. Funct. Mater.* 13, 101 (2003). <http://dx.doi.org/10.1002/adfm.200390014>
- [11] I. Djerdj, D. Arcon, Z. Jaglicic and M. Niederberger, *J. Phys. Chem. C* 111, 3614 (2007). <http://dx.doi.org/10.1021/jp067302t>
- [12] X. Li, L. Zhou, J. Gao, H. Miao, H. Zhang and J. Xu, *Powder Technol.* 190, 324 (2009). <http://dx.doi.org/10.1016/j.powtec.2008.08.010>
- [13] Z. Weixin, W. Cheng, Z. Xiaoming, X. Yi and Q. Yitai, *Solid State Ionics* 117, 331 (1999). [http://dx.doi.org/10.1016/S0167-2738\(98\)00432-9](http://dx.doi.org/10.1016/S0167-2738(98)00432-9)
- [14] N. Wang, L. Guo, L. He, X. Cao, C. Chen, R. Wang and S. Yang, *Small* 4, 606 (2007). <http://dx.doi.org/10.1002/smll.200600283>
- [15] J. Du, Y. Gao, L. Chai, G. Zou, Y. Li and Y. Qian, *Nanotechnology* 117, 4923 (2006). <http://dx.doi.org/10.1088/0957-4484/17/19/024>
- [16] R.D. Zysler and E. Winkler, *Nanotechnology* 18, 158001 (2007). <http://dx.doi.org/10.1088/0957-4484/18/15/158001>
- [17] E. C. Stoner and E. P. Wohlfarth, *Philos. Trans. R. Soc. A* 240, 599 (1948). <http://dx.doi.org/10.1098/rsta.1948.0007>
- [18] (a) L. Neel and *Ann. Geophysics* 5, 99 (1949); (b) W. F. Brown, *Phys. Rev. B* 130, 1677 (1963). <http://dx.doi.org/10.1103/PhysRev.130.1677>
- [19] L. Sicard, J. M. L. Meins, C. Méthivier, F. Herbst and S. Ammar, *J. Magn. Magn. Mater.* 322, 2634 (2010). <http://dx.doi.org/10.1016/j.jmmm.2010.03.016>
- [20] J. Gao, J. Fu, C. Lin, J. Lin, Y. Han, X. Yu and C. Pan, *Langmuir* 20, 9775 (2004). <http://dx.doi.org/10.1021/la049197p>
- [21] J. Dobryszycski and S. Biallozor, *Corros. Sci.* 43, 1309 (2001). [http://dx.doi.org/10.1016/S0010-938X\(00\)00155-4](http://dx.doi.org/10.1016/S0010-938X(00)00155-4)
- [22] M. Bognitzki, H. Q. Hou, M. Ishaque, T. Frese, M. Hellwig, C. Schwarte, A. Schaper, J. H. Wendorff and A. Greiner, *Adv. Mater.* 12, 637 (2000). [http://dx.doi.org/10.1002/\(SICI\)1521-4095\(200005\)12:9<637::AID-ADMA637>3.0.CO;2-W](http://dx.doi.org/10.1002/(SICI)1521-4095(200005)12:9<637::AID-ADMA637>3.0.CO;2-W)
- [23] X. H. Lu, J. Yang, L. Wang, X. J. Yang, L. D. Lu and X. Wang, *Mater. Sci. Eng. A* 289, 241 (2000).
- [24] J. G. Deng, X. B. Ding and Y. X. Peng, *Polymerica* 43, 2179 (2002). [http://dx.doi.org/10.1016/S0032-3861\(02\)00046-0](http://dx.doi.org/10.1016/S0032-3861(02)00046-0)
- [25] J. Zhang, A. L. Barker, D. Mandler and P. R. Unwin, *J. Am. Chem. Soc.* 125, 9312 (2003). <http://dx.doi.org/10.1021/ja036146q>
- [26] G.V. Kurlyandskaya, J. Cunanan, S. M. Bhagat, J. C. Apesteguy and S. E. Jacobo, *J. Phys. Chem. Solids* 28, 1527 (2007). <http://dx.doi.org/10.1016/j.jpccs.2007.03.031>
- [27] S. K. Pillalamarri, F. D. Blum, A. T. Tokuhira and M. F. Bertino, *Chem. Mater.* 17, 5941 (2005). <http://dx.doi.org/10.1021/cm050827y>
- [28] C. Danielle, S. Michelle, A. Ivo and Z. Aldo, *Chem. Mater.* 15, 4658 (2003). <http://dx.doi.org/10.1021/cm034292p>
- [29] Y. Qiu and L. Gao, *J. Phys. Chem. B* 109, 19732 (2005). <http://dx.doi.org/10.1021/jp053845b>
- [30] X. Li and X. Li, G. Wang, *Mater. Chem. Phys.* 102, 140 (2007). <http://dx.doi.org/10.1016/j.matchemphys.2006.11.014>
- [31] K. Huang, Y. Zhang, Y. Long, J. Yuan, D. Han, Z. Wang, L. Niu and Z. Chen, *Chem. Eur. J.* 12, 5314 (2006). <http://dx.doi.org/10.1002/chem.200501527>
- [32] T. Wejrzanowski, R. Pielaszek, A. Opaliniska, H. Matysiak, W. Lojkowski and K. J. Kurzydowski, *Appl. Surf. Sci.* 253, 204 (2006). <http://dx.doi.org/10.1016/j.apsusc.2006.05.089>
- [33] R. Pielaszek, *Appl. Crystallography Proceedings of the XIX Conference, Krakow, Poland*, 43, 2003.
- [34] A. Baykal, N. Bıtrak, B. Ünal, H. Kavas, Z. Durmuş Ş Özden and M. S. Toprak, *J. Alloys Compd.* 502, 199 (2010). <http://dx.doi.org/10.1016/j.jallcom.2010.04.143>
- [35] H. Kavas, Z. Durmus, M. Şenel, S. Kazan, A. Baykal and M. S. Toprak, *Polyhedron* 29, 1375 (2010). <http://dx.doi.org/10.1016/j.poly.2009.12.034>
- [36] Z. Durmus, M. Tomas, A. Baykal, H. Kavas, T. G. Altınkeçiç and M. S. Toprak, *Russ. J. Inorg. Chem.* 55, 1947 (2010). <http://dx.doi.org/10.1134/S0036023610120211>
- [37] Z. Durmus, A. Baykal, H. Kavas and H. Sozeri, *Physica B* (2011). [doi:10.1016/j.physb.2010.12.059](http://dx.doi.org/10.1016/j.physb.2010.12.059).
- [38] Y. Köseoğlu, A. Baykal, M. S. Toprak, F. Gözüak, A. C. Başaran and B. Aktaş *J. Alloys Compd.* 462, 209 (2008). <http://dx.doi.org/10.1016/j.jallcom.2007.08.023>
- [39] F. Gözüak, Y. Köseoğlu, A. Baykal and H. Kavas, *J. Magn. Magn. Mater.* 321, 2170 (2009). <http://dx.doi.org/10.1016/j.jmmm.2009.01.008>

- [40] J. Liu, T. Xua, M. Gong, F. Yu and Y. Fu, *J. Membrane Sci.* 283, 190 (2006). <http://dx.doi.org/10.1016/j.memsci.2006.06.027>
- [41] Y. Xiaotun, X. Lingge, N. S. Choon and C. S. Hardy, *Nanotechnology* 14, 624 (2003). <http://dx.doi.org/10.1088/0957-4484/14/6/311>
- [42] Z. J. Zhang, X. Y. Chen, B. N. Wang and C. W. Shi, *J. Cryst. Growth* 310, 5453 (2008). <http://dx.doi.org/10.1016/j.jcrysgro.2008.08.064>
- [43] R. Tackett and G. Lawes, *Phys. Rev. B* 76, 024409 (2007). <http://dx.doi.org/10.1103/PhysRevB.76.024409>
- [44] a) B. Unal, Z. Durmus, H. Kavas, A. Baykal and M. S. Toprak, *Matter. Phys. Chem.* 123, 184 (2010). <http://dx.doi.org/10.1016/j.matchemphys.2010.03.080>; b) S. Ü. Çelik and A. Bozkurt, *Eur. Polym. J.* 44, 213 (2008). <http://dx.doi.org/10.1016/j.eurpolymj.2007.10.010>
- [45] B. Hallouet, B. Wetzels and R. Pelster, 11 (2007), Article ID 34527.
- [46] L. Salwa, L. Abd-El-Messieh, S. El-Sabbagh and I. F. Abadir, *J. Appl. Polym. Sci.* 73, 1509 (1999). [http://dx.doi.org/10.1002/\(SICI\)1097-4628\(19990822\)73:8<1509::AID-APP20>3.0.CO;2-8](http://dx.doi.org/10.1002/(SICI)1097-4628(19990822)73:8<1509::AID-APP20>3.0.CO;2-8)
- [47] S. Ukishima, M. Iijima, M. Sato, Y. Takahashi and E. Fukada, *Thin Solid Films* 308, 475 (1997). [http://dx.doi.org/10.1016/S0040-6090\(97\)00438-0](http://dx.doi.org/10.1016/S0040-6090(97)00438-0)
- [48] Wenli Qu, Tze-Man Ko, Rohit H. Vora and Tai-Shung Chung, *Polymer*, 42, 6393 (2001). [http://dx.doi.org/10.1016/S0032-3861\(01\)00111-2](http://dx.doi.org/10.1016/S0032-3861(01)00111-2)
- [49] B. Ünal, Z. Durmus, A. Baykal, H. Sözeri, M. S. Toprak and L. Alpsoy, *J. Alloys. Compd.* 505, 172 (2010). <http://dx.doi.org/10.1016/j.jallcom.2010.06.022>
- [50] H. Kavas, Z. Durmus, A. Baykal, A. Aslan, A. Bozkurt and M. S. Toprak, *J. Non-cryst. Solids*, 356, 484 (2010). <http://dx.doi.org/10.1016/j.jnoncrsol.2009.12.022>